

PAPER • OPEN ACCESS

Absorption enhancement by transition metal doping in ZnS

To cite this article: Gautam Gurung *et al* 2019 *Mater. Res. Express* 6 126550

View the [article online](#) for updates and enhancements.



IOP | ebooks™

Bringing together innovative digital publishing with leading authors from the global scientific community.

Start exploring the collection—download the first chapter of every title for free.



PAPER

Absorption enhancement by transition metal doping in ZnS

OPEN ACCESS

RECEIVED
30 September 2019REVISED
22 October 2019ACCEPTED FOR PUBLICATION
12 November 2019PUBLISHED
22 November 2019

Original content from this work may be used under the terms of the [Creative Commons Attribution 3.0 licence](#).

Any further distribution of this work must maintain attribution to the author(s) and the title of the work, journal citation and DOI.

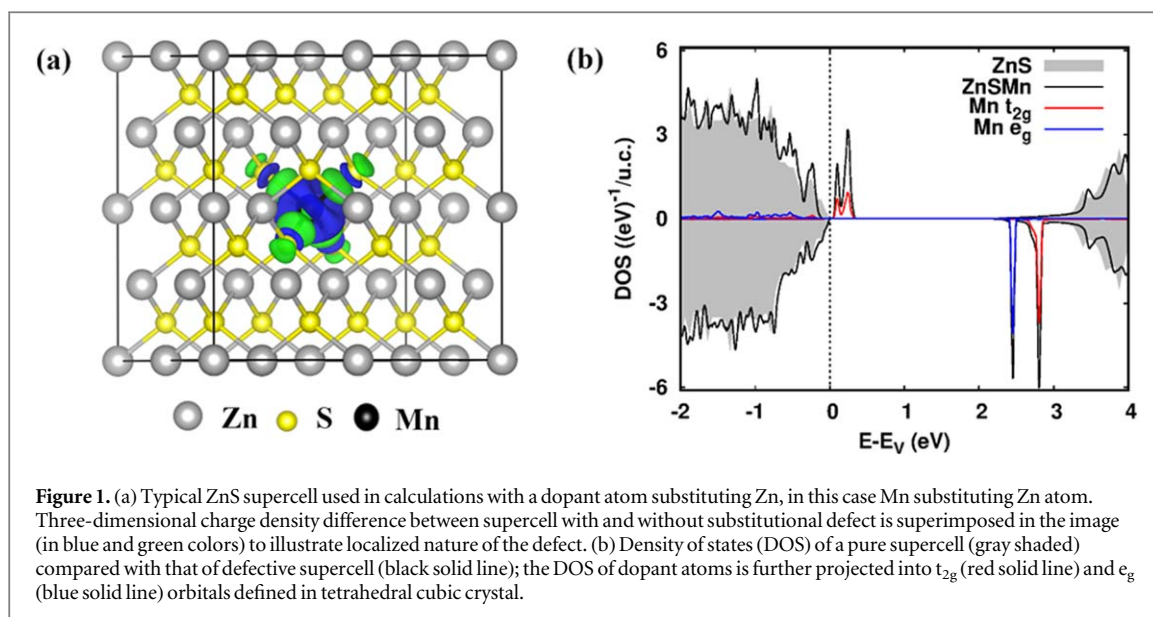
Gautam Gurung¹, Thilini K Ekanayaka¹, Andrew J Yost^{1,2} and Tula R Paudel¹ ¹ Department of Physics and Astronomy & Nebraska Center for Materials and Nanoscience University of Nebraska, Lincoln, Nebraska 68588, United States of America² Department of Physics, Oklahoma State University Stillwater, OK 74078-3072, United States of AmericaE-mail: tpaudel2@unl.edu**Keywords:** ZnS, transition metal doping, absorption enhancementSupplementary material for this article is available [online](#)**Abstract**

Transition metal doping is an effective tool for controlling optical absorption in ZnS and hence the number of photons absorbed by photovoltaic devices. By using first principle density functional calculations, we compute the change in number of photons absorbed upon doping with a selected transition metal and found that Ni offers the best chance to improve the performance. This is attributed to the formation of defect states in the band gap of the host ZnS which give rise to additional dipole-allowed optical transition pathways between the conduction and valence band. Analysis of the defect level in the band gap shows that TM dopants do not pin Fermi levels in ZnS and hence the host can be made n- or p- type with other suitable dopants. The measured optical spectra from the doped solution processed ZnS nanocrystal supports our theoretical finding that Ni doping enhances optical absorption the most compared to Co and Mn doping.

Introduction

Nanostructures, quantum dots and nanocrystals have been long known for their tunable electronic, optical and transport properties. More recently, they have gained renewed interest as they offer ways to fabricate low cost solar cells [1]. However traditional II-V quantum dots solar cells however suffered from low device performance [2, 3]. Transition metal (TM) doping has the potential to improve the absorption properties of low-cost solution prepared transition metal doped ZnS and CdS quantum dots and enhance their photovoltaics efficiency. The quantum dots have large surface to volume ratio, size dependent optical and electronic properties [4–6] and tunable chemical composition and surface morphology. Inclusion of dopants [7] in such systems modifies the band edges and creates mid gap states thereby changing optical and electrical conductivity by providing free carriers or traps. The dopants may also passivate the surface by annulling dangling bonds and increase the stability of low dimensional structures.

ZnS and II-VI semiconductor quantum dots and nanoparticles are easy to synthesize using wet chemistry and their size, crystallinity and structural stability can be controlled by growth temperature. Ability to control virtually every aspect of these materials makes it interesting for several applications including in photovoltaics, photocatalysis, photodetection, linear and non-linear optics, spintronics, plasmonic etc In addition, ZnS based heterostructures [8–10] have gained attention due to design flexibility offered by ZnS. ZnS is less corrosive and can be used with other photovoltaic materials such as CdSe and CdTe in core-shell quantum dot structures and has a large band gap which allows band gap engineering of heterostructure with cascade type band structure for the higher optical absorptions. Further tailoring of the properties is possible by external cation dopants, e.g., Al [11], Mg [12], V [13], Cr [14], Mn [15–20] Fe [21], Co [17, 19, 22], Ni [19, 21–24], Cu [11, 20], Ag [19], Cd [19], Eu [25, 26], Gd [27–29], anion dopants e.g. N and O [30] and co-doping between cation and cation, e.g. Li and Tm [31], Co and Ni [32, 33]; Eu and Mn [34], anion-anion, e.g. N and C [35] and cation-anion co-doping [30]. Additional tuning of properties can be achieved with interlayering with oxides materials, e.g. ZnO [36] which show potentials in imaging, sensing and plasmonic. Fundamental to all these photo-related phenomena is the possibility of using dopants to change the underlying electronic structure and absorption properties. It was



recently shown that even the location of the dopant, either within or at the surface of the quantum dot can influence the electronic properties and photocurrent of the material [37, 38]. To this end, we make use of the first principles density functional theory to study the difference in absorption upon doping ZnS with selected transition metals (TM) namely Mn, Fe, Co, Ni and Au that have their defect states lying near band edge or in the band gap and analyze their absorption properties. Out of these, we find that Ni improves absorption the best and increases output power in the photovoltaic devices. Our findings are supported by the experimental absorbance measurement in the pure ZnS and the TM doped ZnS nanoparticles.

Results and discussions

To study how the defect modifies absorption properties of the host, we construct 64 atoms, $2 \times 2 \times 2$ supercell of conventional Zinc-Blende cubic unit, with a TM atom substituting Zn as shown in figure 1(a). We relax the ions in the supercell keeping its shape fixed until the Hellman–Feynman forces are less than 0.01 eV/\AA to include defect induced relaxation in doped system. In the calculation, we use a kinetic energy cutoff of 340 eV for the plane wave expansion of the PAWs [39] and $4 \times 4 \times 4$ Monkhorst-Pack grid of k points [40] for Brillouin zone integration. In all calculations, we turn on the spin polarization. Transition metals are often multivalent, resulting in non-isoelectronic substitutions with dopant atoms providing more than two electrons to the anions as provided by the host Zn atoms. Such electrons often reside in defect levels and can be removed creating various ionization levels. For example, Mn_{Zn} have three ionization levels: $1+$, 0 , $1-$. To create such ionized (charged) defect, we add to or remove electrons from the system with compensating jellium background. This charge exchange often occurs at the highest occupied state and corresponds to defect ionization. However, in finite supercell addition of charge introduces two complications. The first is that the interaction between the charge and its image, which would not be there if the defect is completely isolated. We take this into account by adding to the total energy a screened Madelung energy resulting from a point charge-image interaction in the lattice compensated by jellium background as suggested by Leslie and Gillan [41] and a screened interaction between the delocalized part of the charge and its image due to Makov and Payne [42]. The dielectric constant that determines screening is calculated using density functional perturbation theory [43] as implemented in VASP. The second complication is the arbitrary shift in the total energy due to additional charge in the system. We correct this shift by calculating a difference in the atomic-sphere averaged electrostatic potentials between the host and charged system [44]. These corrections effectively remove the supercell size dependent energy of a charged system [45] and effectively represent the energy of large, ideally infinite crystal with a single defect (dilute limit), even for the smaller computation cell.

The electronic structure of the supercell with or without defect provides valuable insight to the absorption process. The dopant often produces isolated states deep in the band gap of the ZnS. This is crucial for increasing the dipole allowed optical transition. Figure 1(a) and figure S1-S5 is available online at stacks.iop.org/MRX/6/126550/mmedia, shows the density of states of a TM_{Zn} substitutional defect in the background of the host states. The defect states contain mostly $\text{TM}-t_{2g}$ states, well localized in middle of gap, and arise mainly from $\text{TM}-d$ states in the tetrahedral crystal environments. The localization of this state can also be visualized in real space by

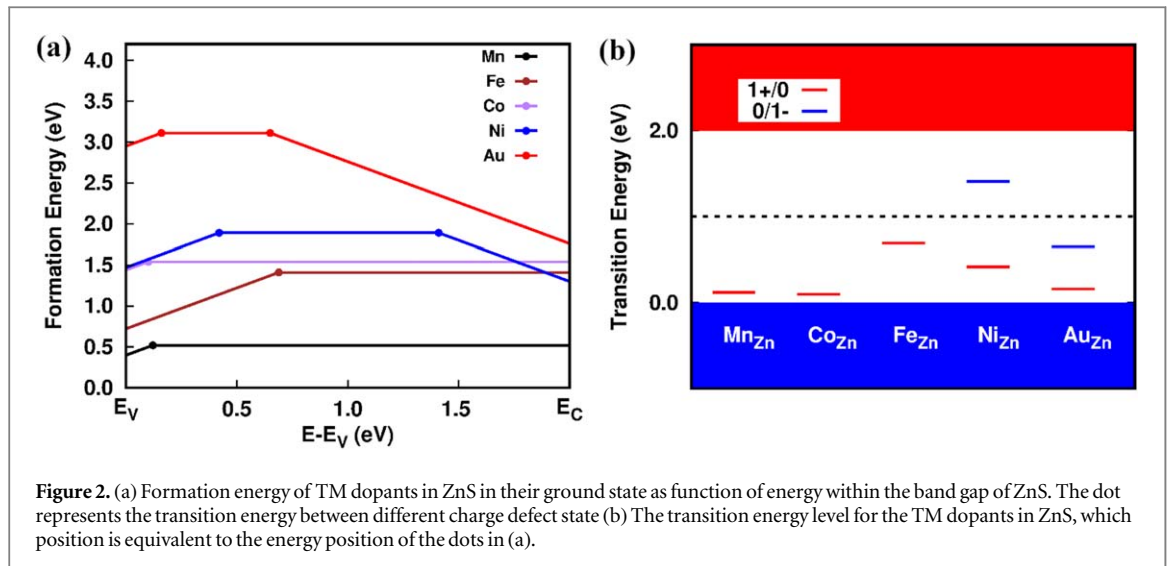


Figure 2. (a) Formation energy of TM dopants in ZnS in their ground state as function of energy within the band gap of ZnS. The dot represents the transition energy between different charge defect state (b) The transition energy level for the TM dopants in ZnS, which position is equivalent to the energy position of the dots in (a).

plotting charge density difference ($\Delta\rho = \rho_D - \rho_{VZn} - \rho_{Mn}$), where ρ_D , ρ_{VZn} and ρ_D are the charge density of supercell with a TM_{Zn} substitutional defect, supercell with a Zn vacancy at the substitutional site and supercell with only one Mn atom at the same position [46] as shown in figure 1 (a). The defect induced charge density is localized in the spherical region with radius equal to distance between next-nearest neighbors. The localization is in-part caused by the relaxation induced by the defect atoms in the host lattice and differs according to a dopants ionization level. For example, the tetrahedral cage around the neutral TM dopant expands for dopants like Mn and Au while it shrinks for the dopants like Ni, Fe, and Co. The charged state 1- compared to the neutral defect state has smaller tetrahedral cage for the magnetic dopants like Mn, Ni, Fe, Co but larger for non-magnetic dopants like Au. The charged state 1+ always has a smaller tetrahedral volume compared to 1- and neutral defect state. The defect level position is found to be qualitatively similar when the calculated band gap of the materials is 2.0 eV in GGA approximation, which is smaller compared to experimental band gap of 3.54 eV or 3.4 eV in HSE06 approximations, thereby indicating reported optical absorption spectra to a large extent is free of band gap underestimation issue ubiquitous in GGA based density functional theory calculations.

All the dopants do not have the same tendency of doping the host materials so that they can bring the changes in optical properties. We determine this tendency by calculating defect formation energy. The formation energy is calculated assuming chemical and charge equilibrium between host and corresponding potentials reservoirs [47] using $HF(D,q,E_F) = E(D,q) - E_H + \mu_{removed} - \mu_{added} + q(E_F - E_V)$ where $E(D,q)$ is the energy of the host with a defect in charge-state q , E_H is the energy without defect, $\mu_{removed}$ and μ_{added} are atomic chemical potentials, E_F is the electron chemical potential (Fermi energy) and E_V is the valence band maximum. The atomic chemical potentials of Fe[body centered cubic(bcc)], Ni[Face centered cubic(fcc)], Zn(hexagonal), Au(fcc), Mn(cubic) and Co(hexagonal) were calculated by considering respective solids in crystal structure given in the bracket.

In figure 2(a), we plot the formation energy of various charge states of TM in ZnS as function of continuously varying Fermi energy across the calculated band gap of the host material. The formation energy of the neutral charge state is independent of the position of the Fermi energy, while it increases for the positively charged donor defects and decreases for negatively charged acceptor defect as fermi energy approaches conduction band from valence band. For all substitutional dopants that we have considered in our study, 1+ charge state is the most favorable one at the valence band maximum. This can be understood in terms of nominal oxidation states of the dopant substituting Zn. All dopants, Mn, Fe, Co, Ni and Au are prevalent in 3+ oxidation state, when they substitute Zn, to a large extent they maintain their characteristics with an extra electron in the defect state that lies close to the valence band. This suggests that when Fermi level of ZnS is fixed to the lower end by an external means, in p-type like conditions, Mn is likely to be found in Mn^{3+} states, which is consistent with the recent experimental prediction based on x-ray Photoelectron spectroscopy study of doped ZnS quantum dot thin films [6]. Additionally, we found that the formation energy of 3d-transition metal substituting Zn is lower than formation energy of 4d- transition metal substituting the Zn.

Furthermore, because of the difference in energy dependence of formation energy of different charge state of a defect, formation of one charge state of a defect is favored over the other at some energy known as transition energy. For example, the formation of neutral charged defect is more favorable over 1+ charge defect when Fermi level is higher than 0.15 eV above the top of valence band for Mn. The transition energy $T(q/q')$ of TM ion in ZnS can be calculated by taking the difference of formation energy and dividing by the charge difference:

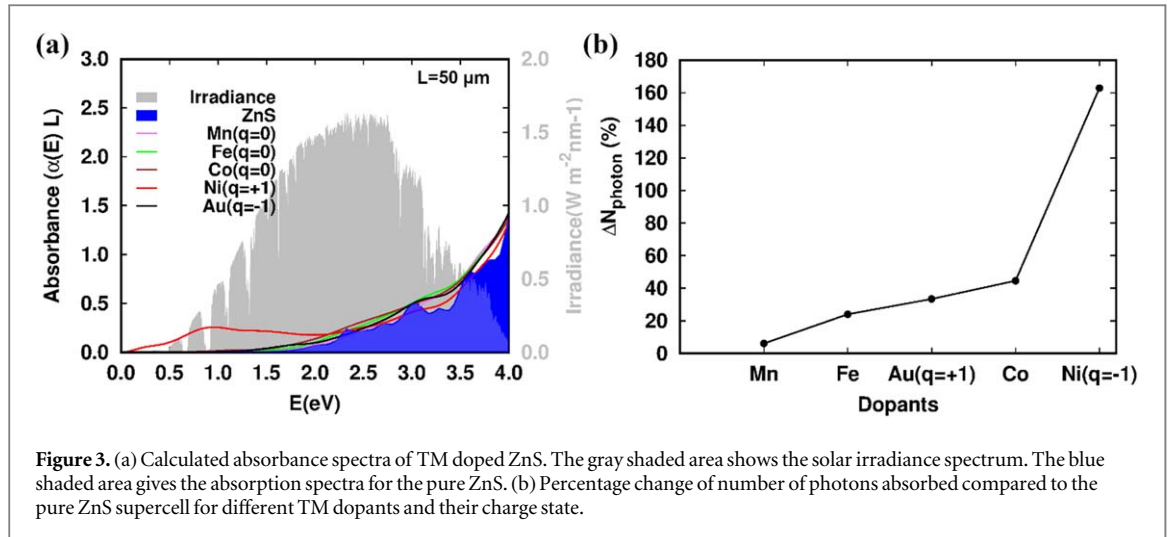


Figure 3. (a) Calculated absorbance spectra of TM doped ZnS. The gray shaded area shows the solar irradiance spectrum. The blue shaded area gives the absorption spectra for the pure ZnS. (b) Percentage change of number of photons absorbed compared to the pure ZnS supercell for different TM dopants and their charge state.

$\{HF(q) - HF(q')\} / (q' - q)$. In figure 2(a), we only show formation energy of the most energetically favorable defect, with the slope of the line indicating the charge state of the defect. The point where the slope of a line changes corresponds to the transition energy $T(q/q')$ above which defect with charge state q becomes energetically favorable over the defect state with charge q' . Alternatively transition energy levels are plotted in figure 2(b) which shows when going up in energy from the top of valence band, 1+ charge state of TM dopants, is energetically favorable up to red line representing 1+/0 transition level. In the middle of gap defect, neutral (0) charge state is favorable until the energy increases above the blue line representing 0/1- charge state. These transition levels lie relatively deep in the band gap, suggesting TM doping may not be as effective as other shallow defects in changing the conduction properties of compounds. Additionally, donor type 0/1+ transition level lies below acceptor type 0/1-. This type of arrangement is categorized as doping type 4 (DT-4) with acceptor above donor [48], the main feature of such kind of defects include absence of Fermi level pinning so that the compound can be made both n-type or p-type by other suitable dopants for example by doping with other intrinsic defects or Zn or S vacancy.

The presence of mid gap states that can both absorb/release electron opens an additional channel for the dipole allowed optical transitions. A density of states plot of neutral defect states (figure S1a to figure S5a) shows that the Fermi level is crossing the defect state in the gap, illustrating such a possibility. Figure 3(a) and figure (S(1-5)d, S(1-5)e, S(1-5)f) shows optical absorption curve for the bulk ZnS and doped ZnS. The absorption spectra were calculated using the energy dependent dielectric function in presence of defect states. The absorption spectra was calculated by using, $\alpha(\omega) = \sqrt{2} \frac{\omega}{c} [\sqrt{\varepsilon_1^2(\omega) + \varepsilon_2^2(\omega)} - \varepsilon_1(\omega)]^{1/2}$, where $\varepsilon_2(\omega)$ is the imaginary part of dielectric constant, which in one-electron picture, $\varepsilon_2(\omega) = \frac{4\pi^2 e^2}{\Omega} \lim_{q \rightarrow 0} \frac{1}{q^2} \sum_{c,v,k} 2w_k \delta(E_c - E_v - \omega) |\langle c|e \cdot \mathbf{q}|v \rangle|^2$, is determined by the integrated optical transitions $\langle c|e \cdot \mathbf{q}|v \rangle$ from the valence states (v) to the conduction states (c), considering the polarization direction (e) of the photon and the electron momentum operator (\mathbf{q}). The integration over the \mathbf{k} is performed by summation over special k-points spanning entire Brillouin zone with corresponding weighting factor w_k . The real part of the dielectric function $\varepsilon_1(\omega)$ is obtained from the imaginary part $\varepsilon_2(\omega)$ using the Kramers-Krönig transformation. Figure S1-S6 shows density of state and absorption spectra associate with each of them. In figure 3(a) we collect absorption spectra from each dopant for the comparison. Absorption spectra of the Ni 1+ charged state stands out among other dopants. In this case, very large empty density of state is located near valence band maxima (figure S4). It is not smeared and remains separate unlike 1+ charged state of Mn and Co. As a result, absorption starts from very small energy ~ 0.1 eV however maximum absorption occurs around 1 eV. Figure S1 shows that the spin down valence band and the defect state are nearly 1 eV separate. So, the maximum absorption can be correlated with the transition between these two states. In neutral charge state, half of the defect state is filled and transition from valence band maximum to the defect state is halved compared to 1+ defect states. In additions, defect state in neutral states are higher in energy due to added electrostatic repulsion with the electrons in the valence band. In 1- charge state, most of the defect state are filled and the optical transition from VBM to defect state is completely suppressed.

To further quantify the effect of the such change in absorption due to defect we calculate the number of photon absorbed [49], by using $N_p = \int_0^\infty a(E) I_{sun}(E) dE$, where $I_{sun}(E)$ is the solar radiation flux and

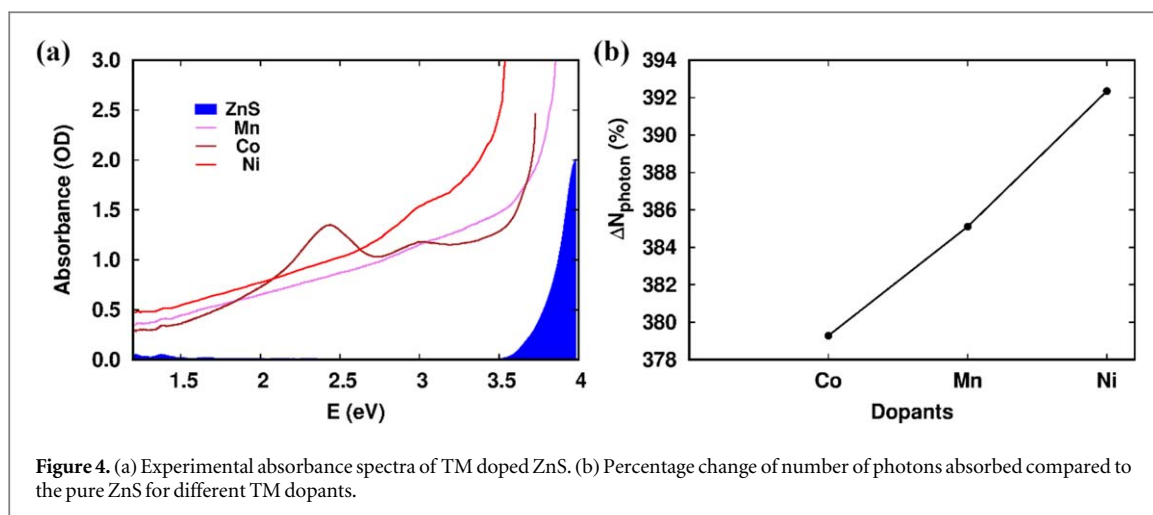


Figure 4. (a) Experimental absorbance spectra of TM doped ZnS. (b) Percentage change of number of photons absorbed compared to the pure ZnS for different TM dopants.

$a(E)$ is the photon absorptivity. The absorptivity is given by $a(E) = 1 - e^{-2\alpha(E)L}$ and depends on the absorption coefficient $\alpha(E)$ and absorber thickness L . For comparison we use typical solar cell thickness $L = 50$ micron assuming thin film geometry [50]. Figure 3(b) shows $\Delta N/N = (N(D) - N)/N$, where N and $N(D)$ are the integrated absorbed photon in absence and presence of defect (D). Ni as expected from its absorption behavior shows greatest change in number of photons absorbed compared to undoped ZnS. This is mainly due to presence of large absorption coefficient in the wide region where solar irradiation intensity is significant compared to the other TM doped ZnS absorption spectra as can be seen in figure 3(a).

The theoretical prediction is qualitatively verified by measured absorbance in TM doped ZnS and doped ZnS quantum dots. ZnS and doped ZnS quantum dots were prepared using a precipitation reaction method. For synthesizing undoped ZnS quantum dots commercial (Sigma Aldrich) Zn acetate ($\text{Zn}(\text{CH}_3\text{COO})_2 \cdot 2\text{H}_2\text{O}$) and Na_2S were used each being 99.999% pure. A solution of 0.1 M of $\text{Zn}(\text{CH}_3\text{COO})_2 \cdot 2\text{H}_2\text{O}$ in dimethyl sulfoxide (DMSO) was prepared by dissolving the $\text{Zn}(\text{CH}_3\text{COO})_2 \cdot 2\text{H}_2\text{O}$ in 40 ml of DMSO. Next 0.5 ml of 1-thioglycerol was added drop wise to the mixture. 1-thioglycerol acts as the capping agent to prevent the agglomeration of quantum dots. The mixture was then heated to 75 °C with constant stirring. A solution of 0.2 M of Na_2S was prepared by dissolving Na_2S in 10 ml of deionized water and was injected to the mixture. The mixture was kept at constant temperature with continuous stirring for 9 h and cooled using an ice bath. Transition metal doped ZnS (Mn:ZnS, Ni:ZnS, Co:ZnS) quantum dots were prepared by adding 10 wt% of dopants Mn (II) acetate $\text{Mn}(\text{CH}_3\text{COO})_2 \cdot 4\text{H}_2\text{O}$, Ni (II) acetate $\text{Ni}(\text{CH}_3\text{COO})_2 \cdot 4\text{H}_2\text{O}$, and Co (II) acetate $\text{Co}(\text{CH}_3\text{COO})_2 \cdot 4\text{H}_2\text{O}$, all $\geq 99.998\%$, with the $\text{Zn}(\text{CH}_3\text{COO})_2 \cdot 2\text{H}_2\text{O}$ to DMSO and followed the same procedure. A non-colloidal solution of both undoped and doped ZnS quantum dot solutions were prepared by adding acetone into the colloidal solutions. The absorption measurements of all the non-colloidal solutions were taken using a DH-2000-BAL deuterium halogen light source (210–1500 nm), HR4000CG-UV-NIR spectrometer (Ocean Optics). The solutions were placed in cuvettes with a path length of 10 mm.

The experimental absorbance spectra for the pure ZnS and the TM doped ZnS nanoparticles is shown in the figure 4(a). Similar to what we find theoretically, experimental measurements also show clear improvement of absorbance upon doping. Additionally, it shows that Ni doping enhances the absorption the most compared to Co, Mn similar to the calculations finding figure 3(b). To further quantify this improvement, we calculate change in number of photons absorbed from experimental absorbance curve assuming it contains all information about the dimensionality of the sample. We rewrite the absorptivity $a(E) = 1 - e^{-2A(E)}$ in terms of absorbance $A(E)$ and calculate the change in number of photons following similar procedure we used in theoretical calculations. Figure 4(b), shows changes in photons absorbed with respect to the pure ZnS; not surprisingly the number of photons absorbed is largest in case of the Ni doping compared to other dopants. While quantitative comparison between theory and experiments is enticing, here we only seek quantitative comparison as we do not include all possible transition pathways that may be available experimentally. For example, Mn doping favors formation of Zn vacancy, which contributes additional states in the band gap which leads to further changes in the absorption spectra. In fact, availability of extra optical transitions pathways may be the reason behind larger changes in photon absorptions in experiments compared to the theory.

Conclusions

In summary, out of Mn, Fe, Co, Ni, Au dopant we considered in Sphalerite ZnS, we found that Ni dopant is most efficient to improve its absorption properties. This is attributed to formation of dipole active states in the band gap of the ZnS. Our finding matches qualitatively with that found in the experiments involving ZnS nanocrystal, showing the possibility of using density functional theory for suitable dopant search for enhancing optical absorption even for the solution processed solar cells devices.

Acknowledgments

This work is supported by the Nebraska Public Power District through the Nebraska Center for Energy Sciences Research at the University of Nebraska-Lincoln, NCESR grant number 19-SE-2018. Computations were performed utilizing the Holland Computing Center at the University of Nebraska. TP and GG acknowledge valuable discussion with Prof Evgeny Y Tsybmal at the University of Nebraska-Lincoln.

ORCID iDs

Tula R Paudel  <https://orcid.org/0000-0002-9952-9435>

References

- [1] Kamat P V 2013 Quantum dot solar cells. The next big thing in photovoltaics *J. Phys. Chem. Lett.* **4** 908–18
- [2] Diguna L J, Shen Q, Kobayashi J and Toyoda T 2007 High efficiency of CdSe quantum-dot-sensitized TiO₂ inverse opal solar cells *Appl. Phys. Lett.* **91** 023116
- [3] Pattantyus-Abraham A G et al 2010 Depleted-heterojunction colloidal quantum dot solar cells *ACS Nano* **4** 3374–80
- [4] Alivisatos A P 1996 Semiconductor clusters, nanocrystals, and quantum dots *Science (80-.)*. **271** 933–7
- [5] Kan S, Mokari T, Rothenberg E and Banin U 2003 Synthesis and size-dependent properties of zinc-blende semiconductor quantum rods *Nat. Mater.* **2** 155–8
- [6] Yost A J et al 2019 Influence of the Cation on the Surface Electronic Band Structure and Magnetic Properties of Mn:ZnS and Mn:CdS *Quantum Dot Thin Films* **123** 24890–24898
- [7] Norris D J, Efros A L and Erwin S C 2008 Doped Nanocrystals *ChemInform* **39** 1776–80
- [8] Zhang J, Zhang Q, Wang L, Li X and Huang W 2016 Interface induce growth of intermediate layer for bandgap engineering insights into photoelectrochemical water splitting *Sci. Rep.* **6** 1–10
- [9] Smith A M, Mohs A M and Nie S 2009 Tuning the optical and electronic properties of colloidal nanocrystals by lattice strain *Nat. Nanotechnol.* **4** 56–63
- [10] Wang X, Yu J and Chen R 2018 Optical characteristics of ZnS passivated CdSe/CdS quantum dots for high photostability and lasing *Sci. Rep.* **8** 1–7
- [11] Nguyen T T, Trinh X A, Nguyen L H and Pham T H 2011 Photoluminescence characteristics of as-synthesized and annealed ZnS:Cu, Al nanocrystals *Adv. Nat. Sci.: Nanosci. Nanotechnol.* **2** 035008
- [12] Shahid M Y, Asghar M, Arbi H M, Zafar M and Ilyas S Z 2016 Role of magnesium in ZnS structure: Experimental and theoretical investigation *AIP Adv.* **6** 025019
- [13] El Amine Monir M et al 2016 Half-metallicity and optoelectronic properties of V-doped zinblende ZnS and CdS alloys *Int. J. Mod. Phys.* **30** 1650034
- [14] Amaranatha Reddy D, Murali G, Vijayalakshmi R P, Reddy B K and Sreedhar B 2011 Effect of Cr doping on the structural and optical properties of ZnS nanoparticles *Cryst. Res. Technol.* **46** 731–6
- [15] Li D, Li L, Liang C J and Niu Y 2011 Energy stabilities, magnetic properties, and electronic structures of diluted magnetic semiconductor Zn_{1-x}MnxS(001) thin films *Chinese J. Chem. Phys.* **24** 47–54
- [16] Peng W Q, Qu S C, Cong G W, Zhang X Q and Wang Z G 2005 Optical and magnetic properties of ZnS nanoparticles doped with Mn²⁺ *J. Cryst. Growth* **282** 179–85
- [17] Savoyant A, D'Ambrosio S, Kuzian R O, Daré A M and Stepanov A 2014 Exchange integrals in Mn- and Co-doped II-VI semiconductors *Phys. Rev. B - Condens. Matter Mater. Phys.* **90** 1–14
- [18] Kole A K and Kumbhakar P 2012 Effect of manganese doping on the photoluminescence characteristics of chemically synthesized zinc sulfide nanoparticles *Appl. Nanosci.* **2** 15–23
- [19] Ramasamy V, Praba K and Murugadoss G 2012 Synthesis and study of optical properties of transition metals doped ZnS nanoparticles *Spectrochim. Acta Part A Mol. Biomol. Spectrosc.* **96** 963–71
- [20] Ummartyotin S, Bunnak N, Juntaro J, Sain M and Manuspiya H 2012 Synthesis and luminescence properties of ZnS and metal (Mn, Cu)-doped-ZnS ceramic powder *Solid State Sci.* **14** 299–304
- [21] Borse P H, Deshmukh N, Shinde R F, Date S K and Kulkarni S K 1999 Luminescence quenching in ZnS nanoparticles due to Fe and Ni doping *J. Mater. Sci.* **34** 6087–93
- [22] Chaurasiya R and Dixit A 2019 Transition metal doped ZnS monolayer: the first principles insights *The Physics of Semiconductor Devices. IWPSD 2017. Springer Proc. in Physics* 49–56
- [23] Yang P et al 2002 Strong green luminescence of Ni²⁺-doped ZnS nanocrystals *Appl. Phys. A Mater. Sci. Process.* **74** 257–9
- [24] Wu M, Wei Z, Zhao W, Wang X and Jiang J 2017 Optical and magnetic properties of Ni Doped ZnS diluted magnetic semiconductors synthesized by hydrothermal method *J. Nanomater.* 1–9
- [25] Horoz S et al 2016 Controlled synthesis of Eu²⁺ and Eu³⁺ doped ZnS quantum dots and their photovoltaic and magnetic properties *AIP Adv.* **6** 045119

- [26] Cheng B C and Wang Z G 2005 Synthesis and optical properties of europium-doped ZnS: long-lasting phosphorescence from aligned nanowires *Adv. Funct. Mater.* **15** 1883–90
- [27] Divya A, Siva Kumar K and Sreedhara Reddy P 2011 Synthesis and characterization of Gd doped ZnS nanoparticles: enhanced photoluminescence properties *Int. Conf. on Nanoscience, Engineering and Technology (ICONSET 2011)* 620–622
- [28] Sanjeev Kumar R et al 2019 Effect of gadolinium doped ZnS nanoparticles: ferro magnetic photocatalyst for efficient dye degradation *SN Appl. Sci.* **1** 268
- [29] Venkatesha N, Poojar P, Qurishi Y, Geethanath S and Srivastava C 2017 Zn $1-x$ Gd x S ($x = 0.1, 0.2$ and 0.3) nanoparticles for magnetic resonance imaging and optical fluorescence imaging *Mater. Res. Express* **4** 035030
- [30] Ma X 2011 Study of the P-type doping properties of ZnS nanocrystals *J. Nanomater.* **2011** 1–5
- [31] Daud A et al 1992 Related content Photoluminescence on Li-Codoped ZnS : Tm Phosphor *Jpn. J. Appl. Phys.* **31** 3383–4
- [32] Zhao W et al 2017 Optical and magnetic properties of Co and Ni co-doped ZnS nanorods prepared by hydrothermal method *J. Alloys Compd.* **698** 754–60
- [33] Yin Z-H and Zhang J-M 2016 Structural, electronic and magnetic properties of the (Co, Ni) codoped ZnS: a first-principles study *Phys. Lett. A* **380** 2796–802
- [34] Chen W, Joly A G, Malm J-O and Bovin J-O 2004 Upconversion luminescence of Eu³⁺ and Mn²⁺ in ZnS:Mn²⁺, Eu³⁺ codoped nanoparticles *J. Appl. Phys.* **95** 667–72
- [35] Sun H, Zhao X, Zhang L and Fan W 2011 Origin of the enhanced visible photocatalytic activity in (N, C)-Codoped ZnS studied from density functional theory *J. Phys. Chem. C* **115** 2218–27
- [36] D'Amico P et al 2017 New energy with ZnS: novel applications for a standard transparent compound *Sci. Rep.* **7** 16805
- [37] Rimal G et al 2016 Giant photocurrent enhancement by transition metal doping in quantum dot sensitized solar cells *Appl. Phys. Lett.* **109**
- [38] Yost A J et al 2017 Effects of Mn dopant locations on the electronic bandgap of PbS quantum dots *Appl. Phys. Lett.* **111**
- [39] Blöchl P E 1994 Projector augmented-wave method *Phys. Rev. B* **50** 17953–79
- [40] Monkhorst H J 1976 Special points fro Brillouin-zone integretions *Phys. Rev. B* **13** 5188–92
- [41] Leslie M and Gillan N J 1985 The energy and elastic dipole tensor of defects in ionic crystals calculated by the supercell method *J. Phys. C: Solid State Phys.* **18** 973–982
- [42] Makov G and Payne M C 1995 Periodic boundary conditions in *ab initio* calculations *Phys. Rev. B* **51** 4014–22
- [43] Baroni S and Resta R 1986 *Ab initio* calculation of the macroscopic dielectric constant in silicon *Phys. Rev. B* **33** 7017–21
- [44] Lany S and Zunger A 2008 Assessment of correction methods for the band-gap problem and for finite-size effects in supercell defect calculations: case studies for ZnO and GaAs *Phys. Rev. B - Condens. Matter Mater. Phys.* **78** 17–20
- [45] Lany S and Zunger A 2009 Accurate prediction of defect properties in density functional supercell calculations *Model. Simul. Mater. Sci. Eng.* **17** 084002
- [46] Zhang R, Lee T and Yu B 2012 The role of titanium nitride supports for single-atom platinum-based catalysts in fuel cell technology w *Phys. Chem. Chem. Phys.* **14** 16552–7
- [47] Zhang S and Northrup J 1991 Chemical potential dependence of defect formation energies in GaAs: Application to Ga self-diffusion *Phys. Rev. Lett.* **67** 2339–42
- [48] Paudel T R, Zakutayev A, Lany S, D'Avezac M and Zunger A 2011 Doping rules and doping prototypes in A₂BO₄ spinel oxides *Adv. Funct. Mater.* **21** 4493–501
- [49] Huang X, Paudel T R, Dong S and Tsymbal E Y 2015 Hexagonal rare-earth manganites as promising photovoltaics and light polarizers *Phys. Rev. B* **92** 125201
- [50] Yu L and Zunger A 2012 Identification of potential photovoltaic absorbers based on first-principles spectroscopic screening of materials *Phys. Rev. Lett.* **108** 1–5